Experimental Validation of Improving Aircraft Rolling Power Using Piezoelectric Actuators

LI Min[1], CHEN Wei-min[2], GUAN De[1], LI Wei[1]

(1. *School of Aeronautics Science and Engineering, Beijing University of Aeronautics and Astronautics, Beijing 100083, China*)

(2. *Division of Engineering Sciences, Institute of Mechanics, CAS, Beijing 100080, China*)

Abstract: Piezoelectric actuators are mounted on both sides of a rectangular wing model. Possibility of the improvement of aircraft rolling power is investigated. All experiment projects, including designing the wind tunnel model, checking the material constants, measuring the natural frequencies and checking the effects of actuators, guarantee the correctness and precision of the finite element model. The wind tunnel experiment results show that the calculations coincide with the experiments. The feasibility of fictitious control surface is validated.

Key words: piezoelectric actuator; rolling power; wind tunnel experiment

利用压电驱动器改善飞机横滚性能的试验验证. 李敏, 陈伟民, 管德, 李维. 中国航空学报(英文版), 2005, 18(2): 108－115.

摘 要:利用分布粘帖在矩形机翼上下两面的压电驱动器,探索使用该类结构提高飞行器横滚能力的可能性。通过风洞模型设计、材料性能测试、模型固有特性测试、压电柔度矩阵测试等试验项目,保证了有限元模型的计算精度,最终通过模型的风洞试验验证了利用气动弹性效应,获得了附加升力与横滚力矩的方案。该原理性试验说明利用分布式压电驱动器改善横滚性能是可行的。

关键词:压电驱动器; 横滚性能; 风洞试验

文章编号: 1000-9361(2005)02-0108-08 **中图分类号**: V217$^+$.33 **文献标识码**:A

Traditionally, a pilot provides a rolling maneuver for turning of the aircraft with an aileron system by rotation of trailing edge control surfaces on the right and left wing in a differential sense. The aileron system increases the lift on one wing and decreases lift on the opposite wing, resulting in a rolling moment producing the rolling maneuver. However, if the aircraft is operating at high dynamic pressures where the deformation of the wing is significant, the rolling rate is reduced until the aileron reversal occurs. The design to avoid aileron reversal will result in increasing the weight of wing.

Recent advancements in actuation and sensing technology have invigorated the exploration of adaptive aerospace structures. In the last 10 years several investigations were conducted to understand the application of smart materials to control of air vehicle structures. The smart materials based actuation system are attractive because of their characteristics high-energy densities. Ehlers and Weisshaar[1] conducted a comprehensive analytical study to understand how active control using piezoelectric (PZT) patches to reshape the wing can improve aerodynamic performance and control static aeroelastic characteristics such as divergence. Lin, Crawley and Heeg[2] conducted a highly innovated experimental and analytical investigations to increase the aircraft flight envelop by suppressing flutter using a distributed network of piezoelectric patches. Richard and Clark[3] further investigated the flutter control of a delta wing. Knot, Eastep, Koloney, *et al*[4-8] published a series of papers about the improvement of aircraft rolling power by using piezoelectric actuators as the struts of the ribs of a wing, and the fictitious control surface (FCS)

Received date: 2004-10-25; Revision received date: 2005-01-26
Foundation item: Aeronautical Science Foundation of China (03A51052); National Defence Preplan(413130308)

technique, using elastic wing twist and camber to achieve a specified rolling rate at all dynamic pressures, was put forward. However, these studies, and several like them[9-11], have shown that a network of sensors and actuators can be used to control a structure and improve the flight performance of air vehicles. NASA and the Defense Advanced Research Projects Agency have adopted the term of "morphing aircraft" to describe the application of the adaptive structures, among other technologies, for this purpose.

The authors[11] adopted a rectangular wing model with distributed piezoelectric actuators. The difference between the model with aileron deflection and the model without aileron was studied. The analytical results showed that these two cases are substantial different. For aileron deflection case, the aeroelastic effect is disadvantageous, so the structural stiffness should be high until the electric voltage is not necessary. But for the case of FCS, the aeroelastic effect is advantageous that means lower structural stiffness can lead to lower voltage. As the subsequent research, in the present investigation a wind tunnel model is designed to validate the calculation results. The ground experiment and the wind tunnel experiment are implemented and the investigations show that the calculation results coincide with the experiment results and the feasibility of FCS is validated.

1 Analytical Models and Equations

1.1 Analytical models

As in Fig.1, a rectangular wing model with aspect ratio 4.0 is used. The analytical model is composed of a number of rectangular aerodynamic panels. The aerodynamic load of each panel is located at 1/4 chord point at mid-span of the panel (pressure point) and the boundary condition is fulfilled at 3/4 chord point at mid-span of the panel (downwash point).

Structurally, the model is a plate with equal thickness, and the piezoelectric plates are bounded on both sides. The structure coordinate is consistent with the aerodynamic coordinate. Finite element model as shown in Fig.2 is constructed by bending plate element with 4 nodes and 5 degrees of freedom for each node. The distribution of piezoelectric plates is consistent with that of aerodynamic panels, as shown in Fig.2.

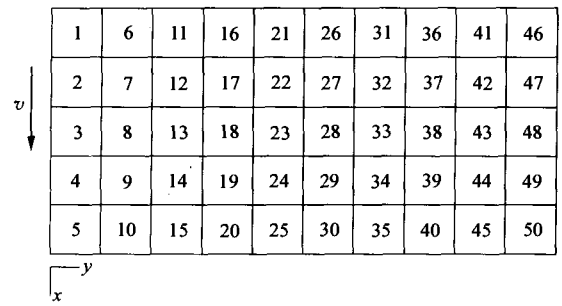

Fig.1 Aerodynamic panels of the wing model

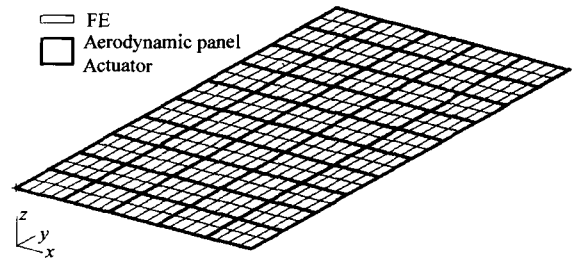

Fig.2 Finite element mode of the wing model

The material of wing model is LY12CZ whose elastic modulus $E_m = 70$ GPa, Poisson ratio $\mu_m = 0.3$ and mass density $\rho_m = 2700$ kg/m^3. The parameters of the piezoelectric actuator used are $E_p = 70$ GPa, $\mu_p = 0.3$ and $\rho_p = 7000$ kg/m^3, and the piezoelectric constants $d_{31} = d_{32}$, being 250×10^{-12} m/V.

1.2 Static aeroelastic equations

The governing equations of static aeroelasticity are as follows:

$$\boldsymbol{\alpha}_f = \boldsymbol{\alpha}_0 + \boldsymbol{\alpha}_e + \boldsymbol{\alpha}_V \tag{1}$$

$$\boldsymbol{\alpha}_f = (\boldsymbol{I} - q\boldsymbol{C}^{\theta z}\boldsymbol{A})^{-1}(\boldsymbol{\alpha}_0 + \boldsymbol{\alpha}_V) \tag{2}$$

$$\boldsymbol{F}_\theta = \boldsymbol{R}\boldsymbol{A}(\boldsymbol{I} - q\boldsymbol{C}^{\theta z}\boldsymbol{A})^{-1}(\boldsymbol{\alpha}_0 + \boldsymbol{\alpha}_V) \tag{3}$$

where $\boldsymbol{\alpha}$ is the column vector of angle of attack of each aerodynamic panel. Subscript 0, e and V denote the initial, elastic deformation and electric voltage of actuator, respectively. $q = \frac{1}{2}\rho_0 v^2$ is the dynamic pressure, ρ_0 is the density of air, v is the velocity of airflow. $\boldsymbol{C}^{\theta z}$ is the flexibility matrix, and

$C_{ij}^{\theta z}$ donates the stream-wise angle at downwash point of the ith aerodynamic panel due to vertical load at pressure point of the jth aerodynamic panel. $\boldsymbol{A}$ is the matrix of aerodynamic force. A_{ij} denotes the lift divided by q on the ith panel due to unit angle of attack at the jth panel. $\boldsymbol{R}$ is a row vector. Set $\boldsymbol{R}=\boldsymbol{I},\boldsymbol{X},\boldsymbol{Y}$, the lift and the aerodynamic moment about y axis or x axis can be obtained. $\boldsymbol{I},\boldsymbol{X}$ and $\boldsymbol{Y}$ represent a row vector of unit, x coordinate and y coordinate of pressure point, respectively.

Aerodynamic force is calculated by horseshoe vortex lattice method[12].

2 Angle of Attack α_V, Rolling Power and Optimization of Voltage Distribution

2.1 Angle of attack $\boldsymbol{\alpha}_V$

The angle of attack α_V induced by piezoelectric force due to voltage is expressed as

$$\boldsymbol{\alpha}_V = (\boldsymbol{C}^{\theta M_x}\boldsymbol{M}_x + \boldsymbol{C}^{\theta M_y}\boldsymbol{M}_y)\boldsymbol{V} \tag{4}$$

where $\boldsymbol{C}^{\theta M_x}$ and $\boldsymbol{C}^{\theta M_y}$ are another flexibility matrices. $C_{ij}^{\theta M_x}$ and $C_{ij}^{\theta M_y}$ denote the stream-wise angle of the ith downwash point due to unit moments about x and y axes applied at the jth node of the actuators. $\boldsymbol{V}$ is the column vector of the applied voltage.

For the ith pair of piezoelectric actuators, as shown in Fig.3, the moments due to unit applied voltage are

$$M_x = d_{32}\frac{E_p}{1-\mu_p}a(t_m + t_p) \tag{5a}$$

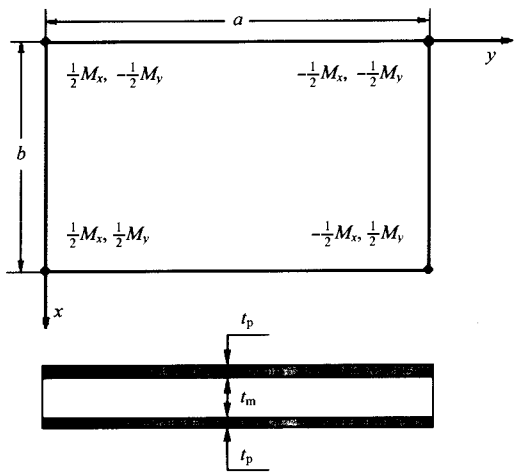

Fig.3 Actuator and related structure

$$M_y = d_{31}\frac{E_p}{1-\mu_p}b(t_m + t_p) \tag{5b}$$

where E_p and μ_p are the elastic modulus and Poisson's ratio of the piezoelectric actuator respectively; t_m and t_p are the thicknesses of the basic plate and actuator respectively; a and b are the length and width of the actuator respectively. M_x and M_y are applied to the nodes of the actuator as shown in Fig.3. As in Fig.1 and Fig.2, each node is related to 1,2 or 4 actuators, so matrices $\boldsymbol{M}_x$ and $\boldsymbol{M}_y$ are constituted by M_x and M_y of the related actuators.

2.2 Rolling power

Rolling rate p is defined by

$$p = \overline{M}_x/\overline{M}_{x,p=1} \tag{6}$$

where $\overline{M}_x$ denotes the rolling moment due to deformation caused by piezoelectric actuator ($\boldsymbol{\alpha}_V$ in Eq. (4)) and deflection of aileron $\boldsymbol{\alpha}_0=[0,\delta]^T$), and $\overline{M}_{x,p=1}$ denotes the rolling moment due to damping when $p=1$ ($\boldsymbol{\alpha}_0 = y/v, \boldsymbol{\alpha}_V = 0$).

2.3 Optimization of voltage distribution

Electrical voltage applied to each actuator is used as design variable. The consumed electric power is used as objective function and should be expressed as

$$W = \sum_{j=1}^{N_P}\frac{1}{2}c_jV_j^2 + \sum_{j=1}^{N_P}\sum_{i=1}^{4}(M_{xj}^i\theta_{xj}^i + M_{yj}^i\theta_{yj}^i)V_j \tag{7}$$

where c_j is the capacitance of the actuator, N_P denotes the number of actuators, M_{xj}^i and M_{yj}^i are the moments about x axis and y axis applied on the ith node of the jth actuator under unit voltage respectively, θ_{xj}^i and θ_{yj}^i are the angles of deflection corresponding to M_{xj}^i and M_{yj}^i respectively. The first item at the right hand side of Eq. (7) represents the energy deposited in actuators, and the second item represents the mechanical work done by voltage applied. The ratio of the second item to W is K^2, named mechanical-electrical coupling constant of piezoelectric actuators. In general, under a fixed work mode the parameter K can be assumed as a constant. In the present investigation, Eq. (8) is used as objective function instead of Eq. (7),

$$W' = \sum_{j=1}^{N_P}\frac{1}{2}c_jV_j^2 \tag{8}$$

The prescribed rolling rate and the maximum value of applied voltage are taken as the constraints. Optimization is conducted by useable feasible direction method[13].

3 Model Design and Analysis Results

A wind tunnel model is designed the to validate the calculation results. Parameters of the model are determined according to the wind tunnel condition, divergence and flutter characters of the model. The model is shown in Fig.4. 200 pieces 40 mm × 20 mm PZT patches are distributed on both sides of a 400 mm × 210 mm rectangular LY12CZ plate without aileron. The thickness of plate and PZT are 3 mm and 0.6 mm respectively. To guarantee stable air, the leading edge of the model is semicircle and the trailing edge is tapering. The composite envelope is used to smooth the contour of the wing model. The completed model is shown in Fig.5 and the size is 400 mm × 211.5 mm × 8.2 mm. All PZT actuators are separated into 25 groups for applying the voltages.

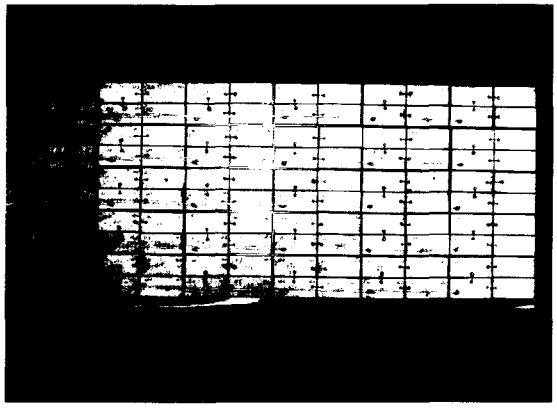

Fig.4 The rectangular wing model with PZT

According to the condition of the wind tunnel, the measurement data are lift and rolling moment. The dynamic pressure of divergence and flutter of this model are listed in Table 1 which shows that the required stiffness is primary from the flutter dynamic pressure. So to guarantee the stability of experimental data, the parameters of experiment are determined as $Ma = 0.7$, dynamic pressure $q = 28\ 420$ Pa and applied voltage 100V/200V/300V/400V.

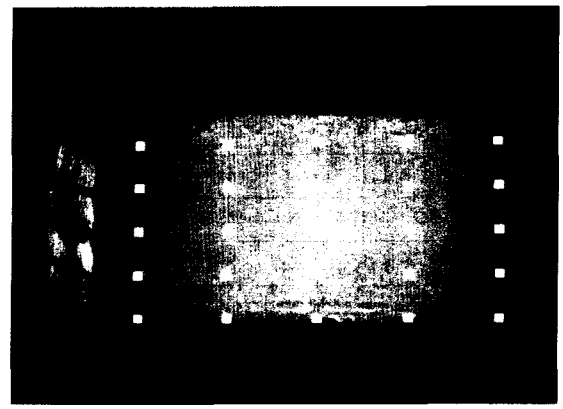

Fig.5 The wing model with composite envelope

Table 1 The flutter and divergence characteristics, Unit: Pa

Ma	q_f	q_d	q_w	q_f/q_w
0.7	47134	76356	28420	1.66

Note: q_f, q_d and q_W represent the dynamic pressure of flutter, divergence and actual data of wind tunnel respective.

4 Ground Experiments

4.1 Checking the material constants

The material constants of plate and PZT, including Young's modulus, yield strength, mass density and piezoelectricity constant (d_{33}, $d_{31} = d_{32}$), are checked by experiments.

The typical displacement curve under applied voltage is shown in Fig.6 which means that the deformation can hold stable. The process from applying the voltage to approximating the stabilization is about 1 s. The displacement will oscillate for reason of suddenly applied voltage, but it can reach the same value when the applied voltage become smooth.

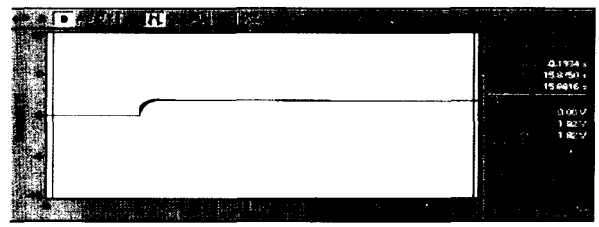

Fig.6 The displacement of the model at the applied voltage

The linear hypothesis of PZT actuating effect is assumed in calculation and the depolarization is very important to select the region of the applied voltage. So lots of experiments on simple model are

implemented to check the linearity of the actuating effect. A serial of voltages varying from −350V to +600 V are applied on a selected actuator, whose thickness is about 0.6 mm, and the deflections of the aluminum plate are recorded (as shown in Fig.7). When positive voltage is applied, the linear region of applied voltage can reach more over 600V. If the voltage is higher than 1000V, the depolarization will occur and the actuating capability of PZT drops rapidly. The same situation would be presented when the negative voltage is applied, but the linearity limit voltage is −350V. In detail, the slope of curve is smaller when the applied voltage is less than 100V. In addition, the deformations in load and unload conditions are not coincident. That means the deformation is related to load path. The maximum difference between the voltage increasing and the decreasing loops is less than 10% (as shown in Fig.8). For a static situation the loop effect is not important. So an approximate linear relationship between displacement and voltage can be assumed in the region of applied voltage in this investigation.

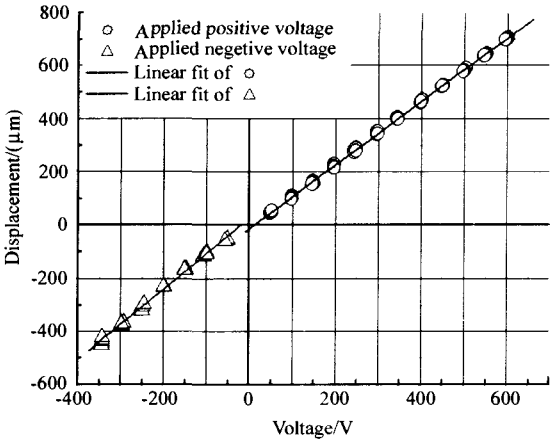

Fig.7 Deflection *vs*. applied voltage

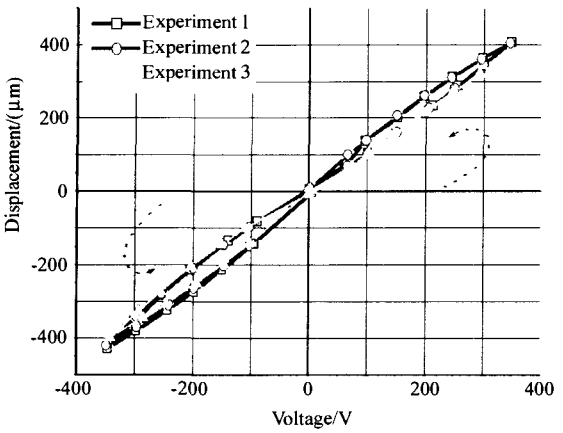

Fig.8 Typical voltage increasing and decreasing loop

4.2 Checking the calculation models

Because of the lower stiffness of the model, the sound excitation and laser measurement are taken to avoid additional stiffness of the measurement system. The laser vibration meter is used to measure the frequencies of the model at various steps. Table 2 lists the calculation and experiment results, including model without the envelope and with the envelope. The relative error between the calculation and the experiment is less than 2%.

Table 2 The natural frequencies of calculation and experiment

	No.1	No.2	No.3	No.4	No.5
Analysis 1	15.6	66.4	96.9	216.0	271.6
Experiment 1	15.3	65.3	96.3	213.0	269.7
Analysis 2	15.4	66.0	96.2	214.6	269.6
Experiment 2	15.3	66.3	96.3	214.7	270.0

Note: 1 and 2 represent the model without envelope and with envelope respectively.

For checking the PZT actuating effect on model, the voltage is applied on actuators at different locations and the deflections are measured at several points (white points in Fig.5). The corresponding calculation is done and the calculation results are compared with the experimental results (shown in Figs. 9-11). In Fig.9 the voltages are applied on actuators at the root chord of the model, and in Fig.10 and Fig.11, at the middle and the tip of the model respectively. In Fig.12 the voltage

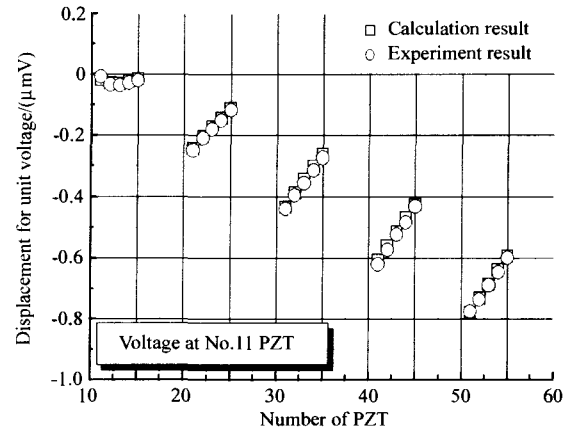

Fig.9 Applied voltage on the PZT at root chord

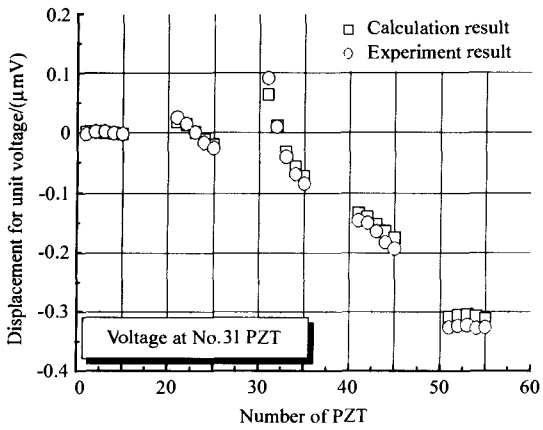

Fig.10 Applied voltage on the PZT at middle chord

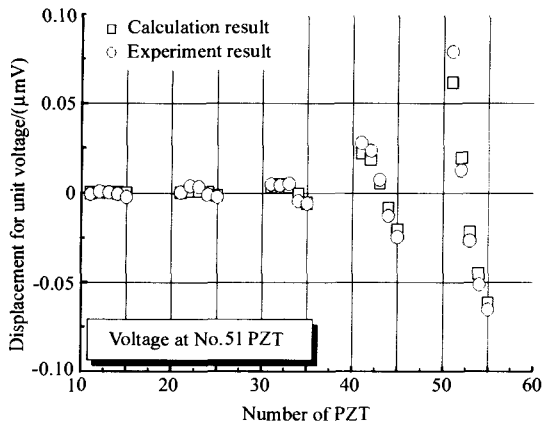

Fig.11 applied voltage on the PZT at tip chord

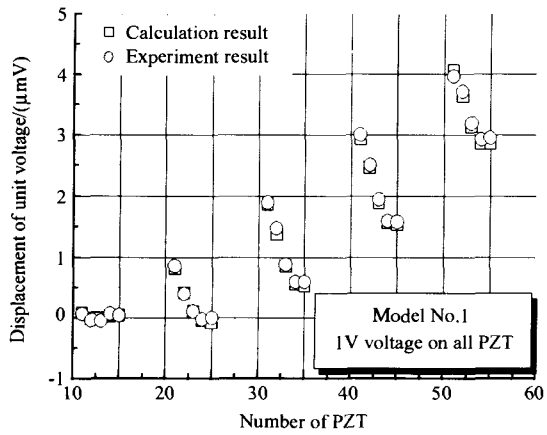

Fig.12 Applied voltage on all PZT

are applied on all actuators. Figs. 9-12 show that both the tendency and the quantity of calculations coincide with those of experiments. As to the group of experimenls in which the voltages are applied at the tip chord, the deformations obtained from experiments are smoother than those obtained from calculations. This may be due to the reason that the concentrated load is employed in calculation.

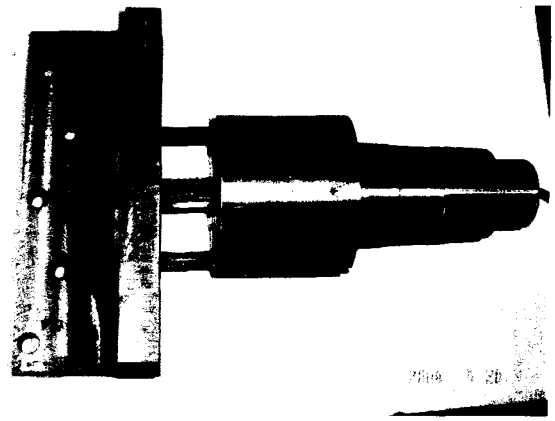

Fig.13 The force balance of wind tunnel

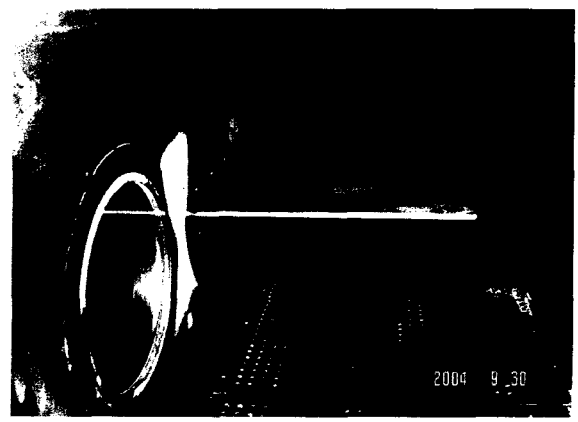

Fig.14 The installation of the wing model

5 Wind Tunnel Experiments

The wind tunnel experiments are implemented in the FL-1 wind tunnel of Institute626. The measuring range of force balance (shown in Fig.13) is 250 N(lift) and 50 N·m (rolling moment). The size of wind tunnel is 600 mm × 600 mm, and the installation of the wing model in wind tunnel is shown in Fig.14. The force balance is fixed on the steel window and only the wing model is in the wind tunnel.

The typical experimental photo is shown in Fig.15, in which it can be seen that the deformation and the angle of attack of the wing model changes with the applied voltages.

In experiments, the Mach number is set to be 0.7 ± 0.0025 and the fluctuation of dynamic pres-

sure is about 3%. The lift and rolling moment are recorded for 10 s with 640 Hz sampling frequency when the dynamic pressure is almost stable.

Fig.15 The typical experimental photo

When the initial angle of attack is 0.5° and no voltage is applied, the comparison between the calculation results and the experiment results is shown in Fig.16, in which the fluctuation of experimental data is induced by the oscillation of dynamic pressure. The lower limit and upper limit of the calculation results are obtained by the minimum and maximum dynamic pressures of the experiment data.

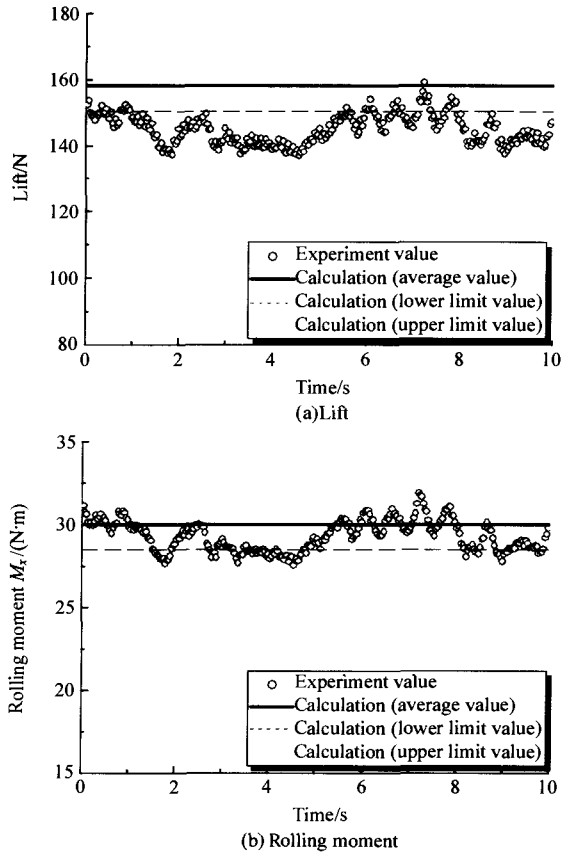

Fig.16 Comparison between calculation, experiment (the initial angle of attack is 0.5°, without applied voltage)

Set the initial angle of attack to be 0°, the lift and rolling moment are recorded as the base data. Then different voltages are applied, and the lift and rolling moment data are recorded once again as shown in Figs.17-18, in which the rolling moment data is relative to the middle point of the force balance.

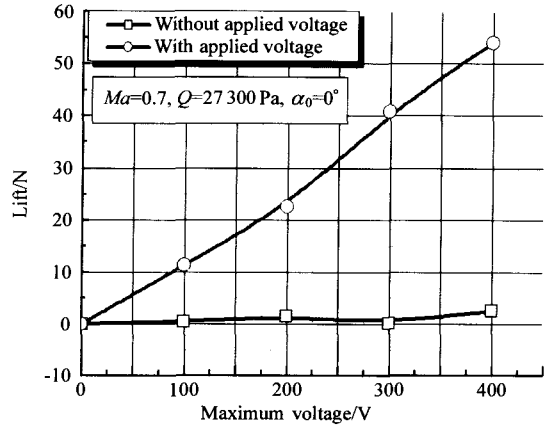

Fig.17 Experimental lift *vs* maximum applied voltage

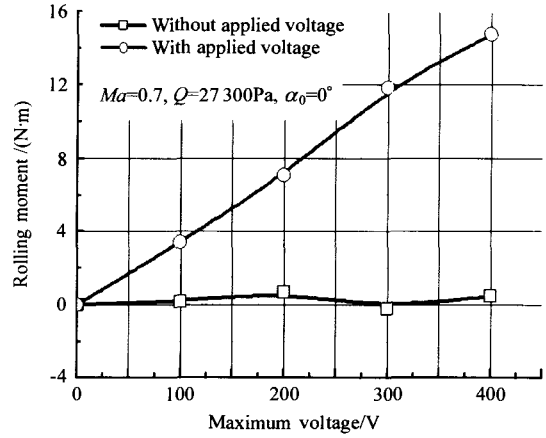

Fig.18 Experimental rolling moment *vs* maximum applied voltage

The comparison between calculation and experiment is shown in Fig.19, in which the rolling moment is translated to the root of the wing model. The experimental result at the maximum applied voltage 400 V is obtained by means of + 500 V and − 300 V for avoiding PZT depolarization. These figures showed that the calculations coincide

with the experiments and the error is less than 10%. The effect of 400 V applied voltage is about equivalent to 0.30° angle of attack of the rigid model.

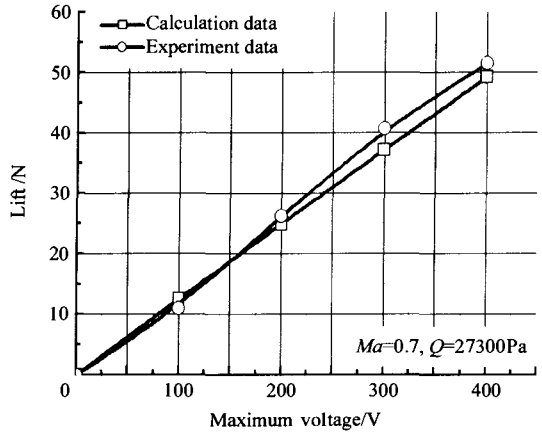

(a) lift

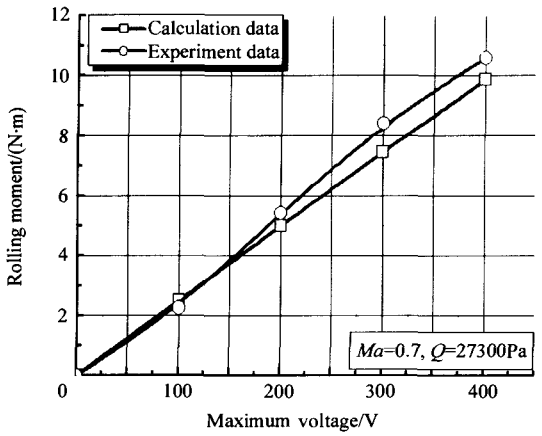

(b) rolling moment

Fig.19 The comparison between the calculation and experiment (the initial angle of attack is 0°)

6 Conclusion Remarks

Piezoelectric actuators are mounted on both sides of a rectangular wing model. The possibility of improvement of aircraft rolling power is investigated. All experiment projects, including designing the wind tunnel model, checking the material constants, measuring the natural frequencies and checking the effects of actuators, guarantee the correctness and precision of the finite element model. The wind tunnel experiment results show that the calculations coincide with the experiments. The feasibility of FCS is validated.

References

[1] Ehlers S M, Weisshaar T A. Static aeroelastic control of an adaptive lifting surface[J]. Journal of Aircraft, 1993,30(4): 534 - 540.

[2] Lin C Y, Crawley E F, Heeg J. Open- and closed-loop results of a strain-actuated active aeroelastic wing[J]. J of Aircraft, 1996, 33(5): 987 - 994.

[3] Richard R E, Clark R L. Delta wing flutter control using spatially optimized transducers[J]. Journal of Intelligent Material System and Structures, 2003, 14: 677 - 691.

[4] Khot N S, Eastep F E, Koloney R M. A method for enhancement of the rolling maneuver of a flexible wing[R]. AIAA-96-1391,1996.

[5] Khot N S, Eastep F E, Koloney R M. Wing twist and camber for the rolling maneuver of a flexible wing without aileron [R]. AIAA-97-1268,1997.

[6] Khot N S, Appa K, Ausman J, *et al*. Deformation of a flexible wing using an active system for a rolling maneuver without ailerons[R]. AIAA-98-1802,1998.

[7] Khot N S, Appa K, Eastep F E. Optimization of flexible wing without ailerons for rolling maneuver[J]. Journal of Aircraft, 2000, 37(5): 892 - 897.

[8] Khot N S, Zweber J V, Veley D E, *et al*. Flexible composite wing with internal actuation for roll maneuver[J]. Journal of Aircraft, 2002, 39(4): 521 - 527.

[9] Sander B, Eastep F E, Forster E. Aerodynamic and aeroelastic characteristics of wings with conformal control surface for morphing aircraft[J]. Journal of Aircraft, 2003, 40(1): 94 - 99.

[10] Sander B, Cowan D, Schere L. Aerodynamic performance of smart wing control effectors[J]. Journal of Intelligent Material System and Structures, 2004, 15: 293 - 303.

[11] Li M, Cheng W M, Guan D. Improvement of aircraft rolling power by use of piezoelectric actuators[J]. Chinese Journal of Aeronautics, 2004, 17(2): 87 - 92.

[12] Hedman S G. Vortex lattice method for calculation of quasi-steady state loadings on thin elastic wings in subsonic flow [R]. FFA Report 105, 1965.

[13] Schmit L A. Structural engineering applications of mathematical programming techniques[R]. AD715483, 1971.

Biographies:

LI Min Associate professor in school of aviation science and engineering, Beijing University of Aeronautics and Astronautics. E-mail: limin@buaa.edu.cn